Synthesis and characterization of α-$SnWO_4$ powders obtained by microwave-assisted hydrothermal method

*M. M. P. Barros[1], K. C. Almeida[1], S. A. Silva[1], G. Botelho[1]**
[1]*Federal University of Tocantins, Department of Environmental Chemistry, 77402-970, Gurupi, TO, Brazil*

Abstract

The structural, morphological, and optical properties of α-$SnWO_4$ synthesized by microwave-assisted hydrothermal method at 150 °C for different times were investigated. XRD revealed the formation of the orthorhombic phase, without the presence of a secondary phase. The sample processed for 64 min showed a reduction in unit cell volume, suggesting a decrease in the structural defects present in the sample. The Raman spectroscopy confirmed the formation of α-$SnWO_4$, with the presence of vibrational modes attributed to the [WO_6] octahedron. FE-SEM images revealed the formation of agglomerate nanosheets in all samples. The band gap (E_{gap}) of the samples presented values in the range from 1.58 to 1.70 eV. The increase in E_{gap} value of the sample processed for 64 min corroborated the decrease in the structural defects suggested by the Rietveld refinement. Finally, the photoluminescence was measured, with maximum emission in the blue region of the electromagnetic spectrum around 454 nm, which was attributed to the [WO_6] octahedron.
Keywords: α-$SnWO_4$, photoluminescence, synthesis, Rietveld refinement.

INTRODUCTION

Tin tungstate ($SnWO_4$) has been highlighted in recent decades due to its unique structural and optical properties, showing potential for applications such as gas-sensing [1, 2], luminescent devices [3, 4], and visible-light-driven photocatalyst [4, 5]. It can be obtained in two different crystalline structures, including the cubic (β-$SnWO_4$) and orthorhombic (α-$SnWO_4$) phases. Both have a low band gap (E_{gap}), with values around 2.68 eV (β-$SnWO_4$) and 1.64 eV (α-$SnWO_4$). The α-$SnWO_4$ is the most studied due to being a low-temperature phase, which was first synthesized by a solid-state reaction in 1972 by Jeitschko and Sleight [6], and, in 1974, its properties were investigated by the same group [7]. The solid-state reaction is a traditional method used in the preparation of α-$SnWO_4$ [8-10], which involves mixing solid reactants and subsequent calcination at high temperatures. Despite its simplicity and low cost, this method has disadvantages, such as non-uniformity of morphology, high agglomeration, large particle size, formation of secondary phases, and lack of reproducibility [11]. To overcome these disadvantages, other processing approaches, such as hydrothermal and microwave-assisted hydrothermal (MAH) methods have been employed to obtain α-$SnWO_4$. For example, nanoplates of α-$SnWO_4$ were prepared with good dispersity by hydrothermal method at 200 °C for 24 h, without any template [12]. Meanwhile, Liu et al. [5] prepared α-$SnWO_4$ nanoparticles with different morphologies (nanostrip to nanosheet) also by hydrothermal method, changing the water/ethylene glycol ratio. Despite the efficiency of the hydrothermal method, long synthesizing times are usually required.

The use of the MAH method for the synthesis of oxides was introduced in 1992 by Komarneni et al. [13]. This method provides a fast and efficient heating approach, which reduces processing time, increases yield, and improves product purity [14]. According to the literature, only one work was found on the preparation of α-$SnWO_4$ using this method [15]. In this work, Su et al. [15] synthesized α-$Sn_{1-x}Zn_xWO_4$ (x=0, 0.02, 0.05, 0.07, 0.10, and 0.12) nanocrystals using a MAH approach at 180 °C for 10 min. This work had the main objective of studying the effects of Zn^{2+} doping on the structural, electronic, and photocatalytic properties of α-$SnWO_4$. However, we have found no research literature detailing the influence of the MAH method on the photoluminescent properties and formation of pure α-$SnWO_4$. Therefore, in our work, the main objective was to study the influence of different exposure times to microwave radiation on the structural, morphological, and optical properties of the α-$SnWO_4$. The α-$SnWO_4$ was obtained by the MAH method at a low temperature (150 °C) for 16, 32, and 64 min. Then, the powders were characterized by X-ray diffraction (XRD), Rietveld refinements, Raman microscopy, field emission gun-scanning electron microscopy (FE-SEM), UV/vis diffuse reflectance spectroscopy (DRS), and photoluminescence spectroscopy (PL).

EXPERIMENTAL

Synthesis of the powders: $SnWO_4$ powders were obtained by the MAH method using different times. Initially, $1x10^{-3}$ mol of tin chloride dihydrate ($SnCl_2.2H_2O$, 98.0% purity, Sigma-Aldrich) and $1x10^{-3}$ mol of sodium tungstate dihydrate ($Na_2WO_4.2H_2O$, 99.0% purity, Sigma-Aldrich) were separately dissolved in 1 and 5 mL of distilled water, respectively. Both solutions were mixed, resulting in a dark-

*gleice.lorena@uft.edu.br
https://orcid.org/0000-0002-7591-1381

red color precipitate. This resulting suspension was diluted to a final volume of 100 mL and then transferred into a Teflon autoclave, that was sealed and placed inside a modified domestic microwave oven of 2.45 GHz of radiation with a maximum output power of 800 W [16]. In the sequence, the suspension was processed at 150 °C for 16, 32, and 60 min, respectively. After microwave processing, the suspension obtained was washed with distilled water and dried in an oven, resulting in a brown-colored precipitate.

Characterization: the samples were characterized by XRD, using a diffractometer (D/Max-2500PC, Rigaku) with CuKα radiation in a scan from 15° to 105° and a scanning speed of 0.02 °/s. The Rietveld refinements were employed, using the General Structure Analysis System (GSAS) software and EXPGUI graphical interface. The following parameters have been refined: scale factor, background modeled using the Chebyshev polynomial of the first kind, shift lattice constants, profile half-width parameters (u, v, w), isotropic thermal parameters, lattice parameters, strain anisotropy factor, and preferential orientation. The peak profile was described by Thompson-Cox-Hastings pseudo-Voigt function. In the refinements, the Inorganic Crystal Structure Database (ICSD) No. 2147 [7] was used. Micro-Raman spectroscopy was performed from 50 to 1300 cm^{-1} using a spectrometer (iHR550, Horiba Jobin-Yvon) coupled to a CCD detector and an argon-ion laser operating at 514 nm. Micrographs of the samples were obtained in a field-emission scanning electron microscope (FE-SEM, Supra 35-VP, Carl Zeiss). The UV/vis diffuse reflectance spectroscopy (DRS) was obtained using a spectrophotometer (Cary 5G, Varian) from 200 to 800 nm. Photoluminescence (PL) measurements were performed with a monochromator (Monospec 27, Thermal Jarrell Ash) coupled to a photomultiplier (R446, Hamamatsu Photonics), with a krypton ion laser (Innova 200 K, Coherent) with emission at λ=350 nm.

RESULTS AND DISCUSSION

Fig. 1a shows the XRD patterns of the $SnWO_4$ powders processed in a MAH for 16, 32, and 60 min. All samples

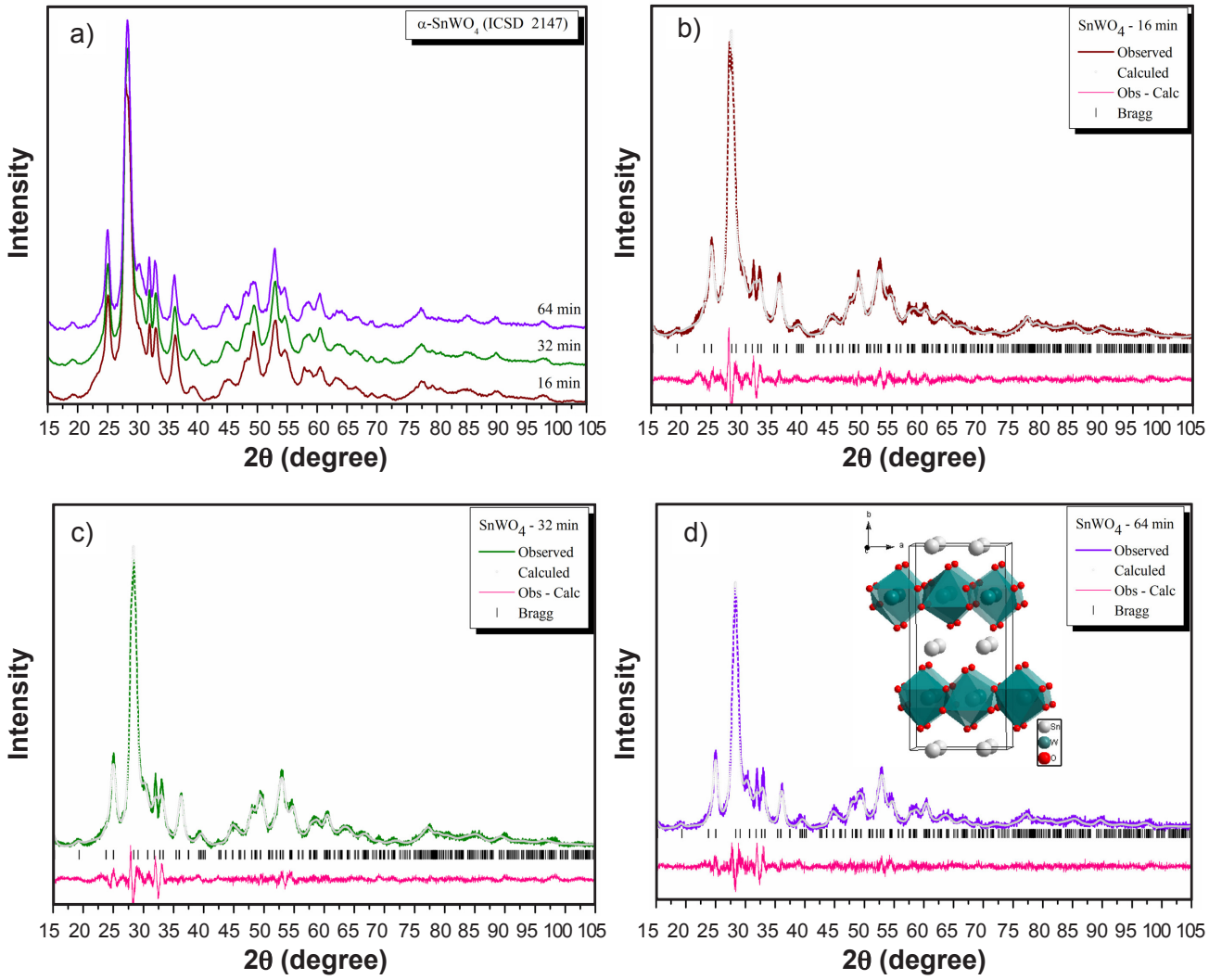

Figure 1: XRD patterns of α-$SnWO_4$ samples (a) and Rietveld refinements plots of α-$SnWO_4$ processed in MAH for 16 min (b), 32 min (c), and 64 min (d). Inset in (d) represents the schematic representation of the orthorhombic structure of α-$SnWO_4$.

Table I - Rietveld refinement results obtained for α-$SnWO_4$ samples.

Sample	Lattice parameter (Å)			Unit cell volume	R_p	R_{wp}	χ^2
	a	b	c	(Å^3)	(%)	(%)	
α-$SnWO_4$ - 16 min	5.5872(1)	11.7865(0)	4.9376(6)	325.16(4)	6.57	8.29	1.48
α-$SnWO_4$ - 32 min	5.5939(3)	11.7555(7)	4.9530(6)	325.71(3)	6.54	8.29	1.51
α-$SnWO_4$ - 64 min	5.5905(1)	11.7185(0)	4.9530(1)	324.48(4)	9.44	11.80	1.18
α-$SnWO_4$ - ICSD 2147	5.6270(3)	11.6486(7)	4.9973(3)	327.56(0)	-	-	-

Table II - Bond lengths results (Å) obtained for α-$SnWO_4$ samples.

Sample	W-O			Sn-O		
α-$SnWO_4$ - 16 min	2.1249(2)	1.7888(2)	1.9032(4)	2.8394(5)	2.3860(3)	2.1755(2)
α-$SnWO_4$ - 32 min	2.1282(2)	1.7918(1)	1.9001(3)	2.8365(4)	2.3867(2)	2.1777(2)
α-$SnWO_4$ - 64 min	2.1270(2)	1.7908(2)	1.8951(4)	2.8302(5)	2.3837(3)	2.1753(2)
α-$SnWO_4$ - ICSD 2147	2.141	1.802	1.889	2.826	2.392	2.184

were well indexed with the orthorhombic structure of α-$SnWO_4$ with space group Pnna, according to the ICSD No. 2147 [7]. The diffractograms have well-defined peaks, indicating a high degree of long-range periodicity; however, the XRD patterns presented broad peaks, suggesting the presence of structural defects arising from the synthesis method and/or the experimental conditions used [17]. The Rietveld refinement method was employed to obtain crystallographic information from the samples. The refinements results (Figs. 1b to 1d) confirmed the formation of the orthorhombic structure of α-$SnWO_4$ without the formation of secondary phases in the samples. The profile acquired by Rietveld refinements (calculated) was in agreement with the experimental profiles (observed), as showed by the residual line (Obs-Calc). This information was supported by the statistical fitting parameters illustrated in Table I (R_p<9.44%, R_{wp}<11.80%, and χ^2 <1.51), which indicated that the quality of refinements was acceptable. In all samples, the values of the lattice parameters and unit cell volume were in accordance with the ICSD Nº 2147 [7] and with the previous reports [5, 9]. The unit cell volume and lattice parameters' values decreased for the sample processed for 64 min, suggesting that the time of exposure to the microwave radiation exerted an effect on the structural parameters of α-$SnWO_4$, decreasing the structural defects present in the sample. Results obtained from the Rietveld refinements were used as input data in the Diamond, a crystal and molecular structure visualization, software to model the schematic representation of the orthorhombic structure of α-$SnWO_4$. As represented in the inset of Fig. 1d, the α-$SnWO_4$ is composed of W coordinated to the six oxygen, arranged in the form of a two-dimensional sheet separated by layers of Sn^{2+} ions, that are also coordinated to six oxygens. The WO_6 clusters within a sheet are connected by four corners. The WO_6 and SnO_6 clusters are highly distorted on the lattice of the α-$SnWO_4$, since there are three different W-O bond lengths and three different Sn-O bond lengths, as illustrated in Table II. The obtained results are in agreement with the ICSD Nº 2147 [7] and with the previous reports [4, 8-10].

Raman spectroscopy was used to complement the structural characterization of the α-$SnWO_4$ samples (Fig. 2). The presence of Raman modes in all samples revealed that the α-$SnWO_4$ presents short-range periodicity, regardless of the processing time. The spectra were very close to previous reports of α-$SnWO_4$, showing a strong Raman mode at approximately 778 cm^{-1}, and three Raman modes of low intensity at approximately 405, 288, and 198 cm^{-1} [8, 18, 19]. Kuzmin et al. [18] attributed the band at 778 cm^{-1} to the stretching O-W-O vibrations of the WO_6 clusters. Moreover, all Raman spectra consisted of wide bands, typically associated with the presence of structural defects.

The morphologies of α-$SnWO_4$ samples were investigated by FE-SEM microscopy (Fig. 3). All samples of α-$SnWO_4$ showed similar morphology, with the formation of highly agglomerated nanosheets with irregular shapes. It is possible to observe that these nanosheets aggregated, forming agglomerates. Wang et al. [20] investigated the

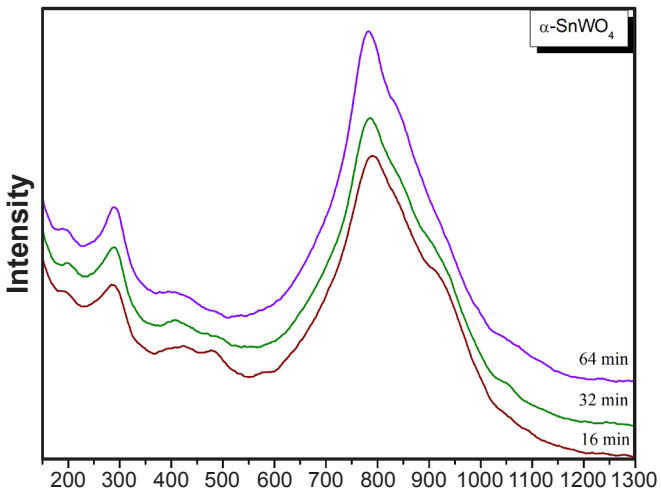

Figure 2: Raman spectra of α-$SnWO_4$ samples.

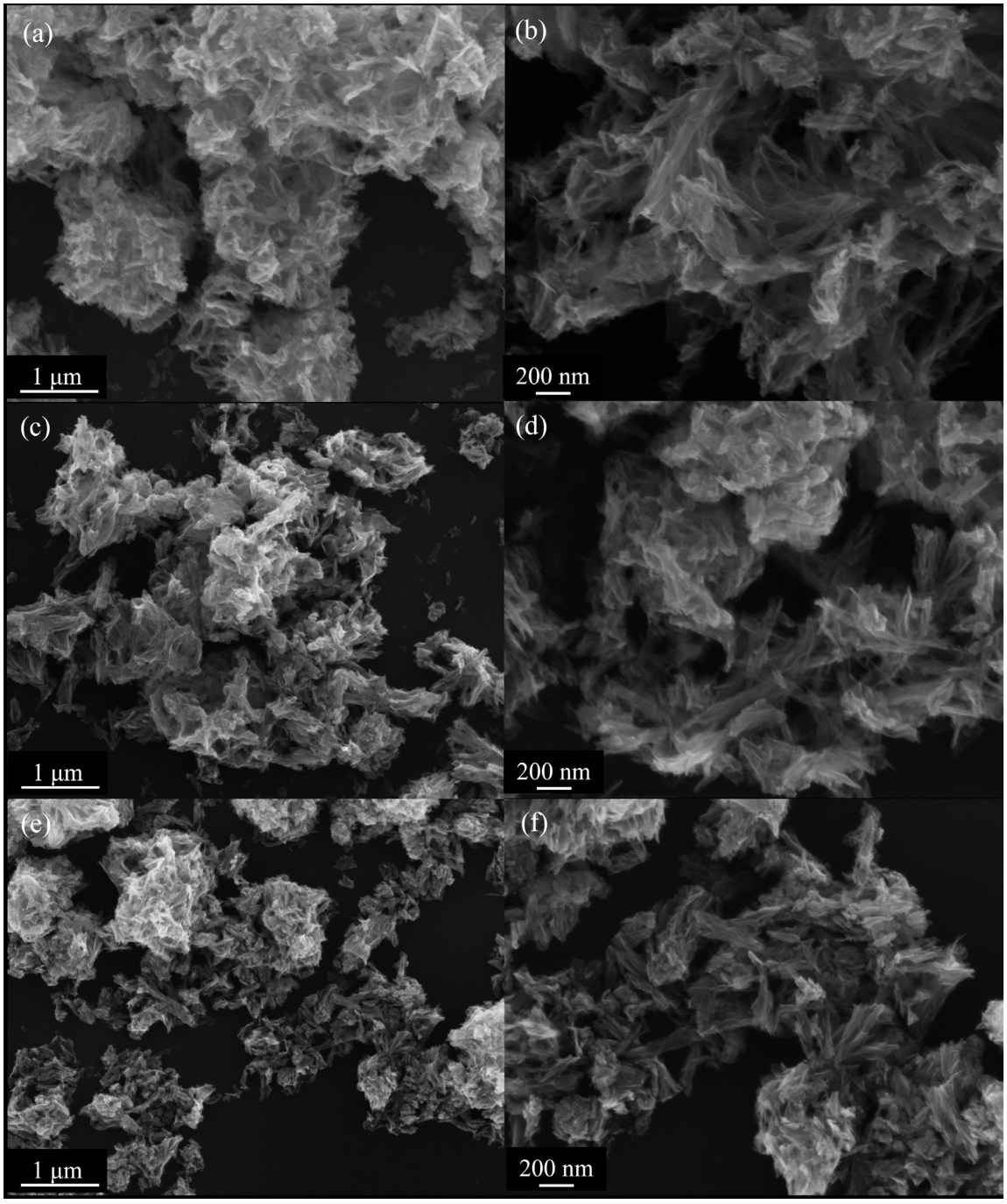

Figure 3: FE-SEM images of α-$SnWO_4$ samples processed for 16 min (a,b), 32 min (c,d), and 64 min (e,f).

morphologies of α-$SnWO_4$ prepared in a different solvent by the solvothermal method. The morphologies showed the formation of nanosheets and agglomerates, suggesting that the solvent is an important factor in tuning the morphology. The α-$SnWO_4$ obtained using only water as solvent presented well-defined nanosheets. The high agglomeration of particles observed in our study may be related to the processing of the sample, under microwave radiation. The microwave radiation accelerates the nucleation and growth process, favoring the aggregation of the particles [17]. Similar morphology of α-$SnWO_4$ was observed in previous studies [4, 15].

To estimate the band gap (E_{gap}) of the samples, the Tauc equation $[\alpha h\nu=A(h\nu-E_{gap})^n]$ [21] was employed, where α is the absorption coefficient, h the Planck constant, ν the frequency, A is a proportionality constant, and the exponent n a constant that depends on the type of electronic transition present in the semiconductor. The absorption coefficient is proportional to the Kubelka-Munk function $[F(R_\infty)]$, resulting in the equation $[F(R_\infty)h\nu]^{1/n}=A(h\nu-E_{gap})$ [22]. According to the previous reports, the $SnWO_4$ powders present an indirect allowed transition with n=2 [5, 9, 20, 23]. Then, the E_{gap} of the samples was obtained by extrapolating the plots of

$[F(R_\infty)h\nu]^{1/2}$ versus hν (photon energy). Fig. 4 shows the E_{gap} of the samples processed at different times. The E_{gap} value increased for the sample processed for 64 min, indicating a reduction in the structural defects with increasing processing time, which was in accordance with the results observed in the Rietveld refinements (Table I). Moreover, these band gap values were in accordance with the previous reports of α-$SnWO_4$, which typically have values in the range of 1.53-1.76 eV [5, 9, 20, 23].

Fig. 5 shows the photoluminescence (PL) spectra of the α-$SnWO_4$ processed for different durations of time. All samples showed a broad emission band, associated with the multi-photon process, with a maximum at around 454 nm (blue region of the electromagnetic spectrum); however, the sample processed for 16 min presented an additional weak emission from 590 to 732 nm. Other metal tungstates, such as Ag_2WO_4, showed a similar emission in the blue and red regions [24, 25]. For example, Longo et al. [24] associated the emission centered at 449 nm with the distorted [WO_6] octahedra, while emission from 621 to 640 nm was associated with the lattice modifier with different coordination and the

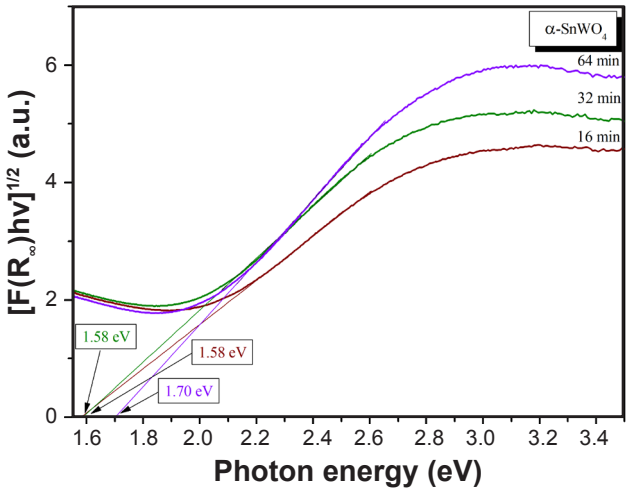

Figure 4: Graph showing the determination of band gap energy of α-$SnWO_4$ samples.

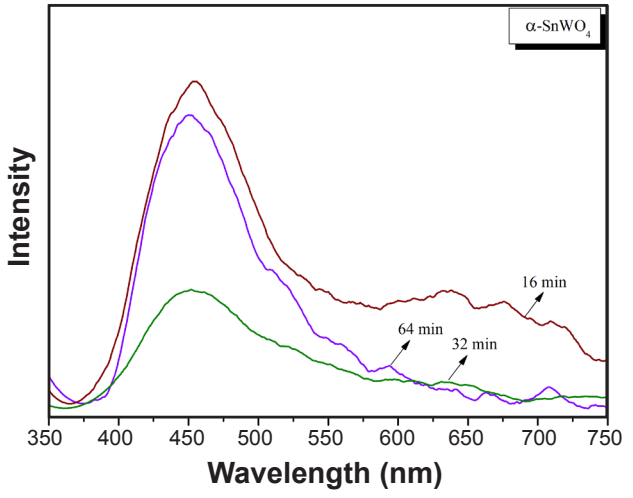

Figure 5: PL spectra of α-$SnWO_4$ samples.

presence of deep levels within the band gap, favoring the red emission. Therefore, we attributed the emission at around 454 nm present in all samples to the distorted WO_6 clusters of the α-$SnWO_4$, as observed in other studies on the PL properties of α-$SnWO_4$ [3, 4]. And the red emission observed in the sample processed for 16 min can be associated with a high concentration of defects resulting from the short processing time. It can also be seen in Fig. 5 that the PL emission of the sample processed for 32 min presented the lowest intensity, which can be associated with several factors, such as the formation of different structural defects resulting from the MAH method, aggregation and orientation of the particles, morphology, and surface defects [17].

CONCLUSIONS

The α-$SnWO_4$ was successfully synthesized by the microwave-assisted hydrothermal (MAH) method, even using low temperature (150 °C) and short processing times (16, 32, and 64 min), showing the efficiency of microwave heating. The XRD and Rietveld refinements confirmed the formation of the orthorhombic phase, composed of highly distorted WO_6 and SnO_6 clusters. The increase in microwave processing time led to slight lattice contraction, suggesting a decrease in the structural defects. This observation was corroborated by the increase in E_{gap} values observed with the increase in processing time. The morphology composed of agglomerated nanosheets was maintained in all samples. The photoluminescence (PL) emission was observed in the blue region in all samples, which was attributed to the WO_6 cluster. These results showed that synthesis methods and processing conditions directly influence the structural, optical, and morphological properties of the α-$SnWO_4$.

ACKNOWLEDGMENTS

The authors acknowledge the CNPq, and Liec-CDMF-UFSCar.

REFERENCES

[1] J. Solis, V. Lantto, Phys. Scr. **T69** (1997) 281.
[2] H. Dong, Z. Li, Z. Ding, H. Pan, X. Wang, X. Fu, Sens. Actuators B Chem. **140**, 2 (2009) 623.
[3] A.P. Chowdhury, B.H. Shambharkar, Adv. Chem. Eng. **4** (2020) 100040.
[4] F.A. Alharthi, M. Shashank, J. Shashikanth, R. Viswantha, A.A. Alghamdi, J. Algethami, M.A. Alsaiari, M.S. Jalalah, N. Ganganagappa, Ceram. Int. **47**, 7 (2021) 10242.
[5] X. Liu, B. Liang, J. Yang, W. Li, J. Taiwan Inst. Chem. Eng. **95** (2019) 575.
[6] W. Jeitschko, A.W. Sleight, Acta Crystallogr. B Struct. Sci. Cryst. Eng. Mater. **28**, 11 (1972) 3174.
[7] W. Jeitschko, A.W. Sleight, Acta Crystallogr. B Struct. Sci. Cryst. Eng. Mater. **30**, 9 (1974) 2088.
[8] J.L. Solis, J. Frantti, V. Lantto, L. Haggstrom, M. Wikner, Phys. Rev. B **57**, 21 (1998) 13491.

[9] I.-S. Cho, C.H. Kwak, D.W. Kim, S. Lee, K.S. Hong, J. Phys. Chem. C **113**, 24 (2009) 10647.
[10] A. Kuzmin, A. Anspoks, A. Kalinko, J. Timoshenko, R. Kalendarev, Phys. Scri. **89**, 4 (2014) 44005.
[11] S. Ivanov, in "Science and technology of atomic, molecular, condensed matter & biological systems", **2**, T.P. Das, B. Sanyal, O. Eriksson (Eds.), Elsevier (2012) 163.
[12] Z. Zhu, H. Tian, M. Zhang, B. Liang, W. Li, Ceram. Int. **42**, 13 (2016) 14743.
[13] S. Komarneni, R. Roy, Q.H. Li, Mater. Res. Bull. **27**, 12 (1992) 1393.
[14] M. Baghbanzadeh, L. Carbone, P.D. Cozzoli, C.O. Kappe, Angew. Chem. Int. Ed. **50**, 48 (2011) 11312.
[15] Y. Su, L. Hou, C. Du, L. Peng, K. Guan, X. Wang, RSC Adv. **2**, 15 (2012) 6266.
[16] E.L. da Silva, J.A. Varela, D.K.A. Almeida, D.P. Volanti, "Microwave aided device for hydrothermal synthesis of nanostructured oxides, particularly obtaining particles of metal oxides, comprises container, in which hydrothermal reaction takes place, and lid for container", Brazil. Patent, BR200815393-A2 (2010).
[17] G. Botelho, J.C. Sczancoski, J. Andres, L. Gracia, E. Longo, J. Phys. Chem. C **119**, 11 (2015) 6293.
[18] A. Kuzmin, M. Zubkins, R. Kalendarev, Ferroelectrics **484**, 1 (2015) 49.
[19] R. Huang, H. Ge, X. Lin, Y. Guo, R. Yuan, X. Fu, Z. Li, RSC Adv. **3**, 4 (2013) 1235.
[20] Q. Wang, H. Li, H. Jiang, S. Ding, Z. Song, J. Shi, Mater. Technol. **30**, 5 (2015) 288.
[21] D. Wood, J. Tauc, Phys. Rev. B **5**, 8 (1972) 3144.
[22] L. Tolvaj, K. Mitsui, D. Varga, Wood Sci. Technol. **45**, 1 (2011) 135.
[23] S. Yao, M. Zhang, J. Di, Z. Wang, Y. Longa, W. Li, Appl. Surf. Sci. **357** (2015) 1528.
[24] E. Longo, D.P. Volanti, V.M. Longo, L. Gracia, I.C. Nogueira, M.A.P. Almeida, A.N. Pinheiro, M.M. Ferre, L.S. Cavalcante, J. Andres, J. Phys. Chem. C. **118**, 2 (2014) 1229.
[25] M. Mondego, R.C. de Oliveira, M. Penha, M.S. Li, E. Longo, Ceram. Int. **43**, 7 (2017) 5759.
(Rec. 24/09/2021, Rev. 05/01/2022, 15/02/2022, Ac. 21/02/2022)